Cancer Research

PINK1 Is a Negative Regulator of Growth and the Warburg Effect in Glioblastoma

Sameer Agnihotri[1,2], Brian Golbourn[1], Xi Huang[1,3,4,5], Marc Remke[1], Susan Younger[3,4,5], Rob A. Cairns[6], Alan Chalil[1], Christian A. Smith[1], Stacey-Lynn Krumholtz[1], Danielle Mackenzie[1], Patricia Rakopoulos[1], Vijay Ramaswamy[1], Michael S. Taccone[1], Paul S. Mischel[7], Gregory N. Fuller[8], Cynthia Hawkins[1,9], William L. Stanford[10], Michael D. Taylor[1], Gelareh Zadeh[1,4,11,12], and James T. Rutka[1,13,14]

Abstract

Proliferating cancer cells are characterized by high rates of glycolysis, lactate production, and altered mitochondrial metabolism. This metabolic reprogramming provides important metabolites for proliferation of tumor cells, including glioblastoma. These biological processes, however, generate oxidative stress that must be balanced through detoxification of reactive oxygen species (ROS). Using an unbiased retroviral loss-of-function screen in nontransformed human astrocytes, we demonstrate that mitochondrial PTEN-induced kinase 1 (PINK1) is a regulator of the Warburg effect and negative regulator of glioblastoma growth. We report that loss of PINK1 contributes to the Warburg effect through ROS-dependent stabilization of hypoxia-inducible factor-1A and reduced pyruvate kinase muscle isozyme 2 activity, both key regulators of aerobic glycolysis. Mechanistically, PINK1 suppresses ROS and tumor growth through FOXO3a, a master regulator of oxidative stress and superoxide dismutase 2. These findings highlight the importance of PINK1 and ROS balance in normal and tumor cells. PINK1 loss was observed in a significant number of human brain tumors including glioblastoma ($n > 900$) and correlated with poor patient survival. PINK1 overexpression attenuates *in vivo* glioblastoma growth in orthotopic mouse xenograft models and a transgenic glioblastoma model in *Drosophila*. *Cancer Res; 76(16); 4708–19. ©2016 AACR.*

Introduction

Glioblastoma is the most common and lethal of all gliomas, with an average survival of approximately 12 to 16 months (1, 2). Activated Ras signaling through receptor tyrosine kinase activation and loss of p53 are two critical glioblastoma alterations that drive tumor formation in both the human disease and murine glioblastoma models (3, 4). These pathways and novel alterations that were previously unknown in glioblastoma have been further validated by The Cancer Genome Atlas (TCGA; refs. 4, 5). However, the vast majority of these alterations are likely to be passengers, alterations that don't contribute to the development of cancer. Functional genomic strategies have been routinely used to identify genes important in driving cancer initiation, progression, and therapeutic resistance, which ultimately complements large-scale sequencing strategies. Implementation of gene insertion strategies, including the sleeping beauty transposon method, have led to the identification of several novel cancer genes (6–8). We hypothesize that nontransformed astrocytes harboring alterations in relevant glioblastoma pathways, including the Ras or p53 signaling, can be transformed using random retroviral insertions to inactivate genes involved in initiation and or progression.

Using a retroviral screen, we identified PTEN-induced Kinase 1, *PINK1*, as a negative regulator of numerous cellular processes exploited in tumor cells. PINK1 is a mitochondrial serine/threonine kinase that is mutated in patients with familial Parkinson disease and regulates several biological functions ranging from mitophagy to reactive oxygen species (ROS) production and oxidative phosphorylation (9–11). It is well understood that deregulation of tumor-suppressor genes and oncogenes frequently affect intracellular ROS levels (12, 13). Cancer cells are constantly challenged by the need to balance oxidative stress and control ROS levels as ROS exerts both pro- and anti-growth effects in cancer (14). We report that PINK1 inhibits glioblastoma

[1]The Arthur and Sonia Labatt Brain Tumor Research Centre, Hospital for Sick Children, Toronto, Ontario, Canada. [2]The Arthur and Sonia Labatt Brain Tumor Research Centre, Hospital for Sick Children, Toronto, Ontario, Canada. [3]Department of Physiology, Howard Hughes Medical Institute, University of California, San Francisco, California. [4]Department of Biophysics, Howard Hughes Medical Institute, University of California, San Francisco, California. [5]Department of Biochemistry, Howard Hughes Medical Institute, University of California, San Francisco, California. [6]Princess Margaret Cancer Centre, University Health Network, Toronto, Ontario, Canada. [7]Ludwig Institute for Cancer Research, University of California, San Diego, California. [8]Department of Pathology, The University of Texas MD Anderson Cancer Center, Houston, Texas. [9]Department of Pathology, Hospital for Sick Children, Ontario, Canada. [10]Sprott Center for Stem Cell Research, Regenerative Medicine Program, Ottawa Hospital Research, Ontario, Canada. [11]Department of Neurosurgery, Toronto Western Hospital, Ontario, Canada. [12]Gelareh Zadeh, University Health Network, Toronto, Ontario, Canada. [13]RS McLaughlin, Professor and Chairman, University of Toronto, Toronto, Ontario, Canada. [14]Department of Surgery, Hospital for Sick Children, Ontario, Canada.

S. Agnihotri and B. Golbourn contributed equally to this article.

G. Zadeh and J.T. Rutka share co-senior authorship of this article.

Corresponding Author: James T. Rutka, The Hospital for Sick Children, Suite 1503, 555 University Avenue, Toronto, Ontario M5G 1×8, Canada. Phone: 416-813-6425; Fax: 416-813-4975; E-mail: james.rutka@sickkids.ca

doi: 10.1158/0008-5472.CAN-15-3079

growth by regulating mitochondrial oxidative phosphorylation, aerobic glycolysis, and ROS.

Materials and Methods

Cell cultures

Astrocyte cultures were established and characterized as previously described from $p53^{-/-}$ (1 week), NMA-P0 (CD1 mice; ref. 7). Fetal human astrocytes were obtained from Lonza. U87 and T98G cell lines were obtained from the ATCC. SF188 cells were a kind gift from Dr. Chris Jones (Institute of Cancer Research, London, United Kingdom). All cells have been previously characterized and authenticated by short tandem repeat profiling in 2011. Cell lines were grown in DMEM (Wisent Technologies) and supplemented with 10% FBS (Wisent Technologies). Glioma stem cells were grown in medium as previously described (15).

Oxygen consumption and glycolytic flux assays

Measurement of oxygen consumption was performed using a Seahorse XF96 analyzer (Seahorse Bioscience). Cells were cultured in their usual growth medium and were reseeded in XF96 plates (30,000 cells) with un-buffered medium. Cells were equilibrated to the un-buffered medium for 90 minutes at 37°C in a CO_2-free incubator before being transferred to the XF96 analyzer. We measured the basal OCR, and then sequentially injected 1.2 μmol/L oligomycin (Sigma), 1.0 μmol/L FCCP (Sigma), and 1.0 μmol/L Rotenone (Sigma; see figures for injection times). Extracellular acidification rate (ECAR) as a measure of glycolytic flux was measured by mpH/min by the Seahorse XF96 analyzer.

Western blot analysis and IHC

Western blots analysis and IHC were carried out as previously described (16). Antibodies were used at the following dilutions: Beta-actin (Sigma-Aldrich Inc., cat. #A2228, 1:10,000), PINK1 (Novus, 1:1,000), Cysteine Sulfenic Acid (Millipore cat. #07-2139, 1:1,000), HIF1A (BD Biosciences, cat. #610958, 1:1,000), PKM2 (Cell Signaling Technology, cat. #4053, 1:1,000), vinculin (Cell Signaling Technology, cat. #4650, 1:1,000), V5 (cat. #Ab9116,1:1,000), PDHK1 (Cell Signaling Technology, cat. #3820, 1:1,000), Phospho PDHE1a (Abgent, cat. #ABCA0122880, 1:1,000), PDHE1a (Santa Cruz Biotechnology, cat. #sc-292543, 1:200), HK2 (Cell Signaling Technology, cat. #2867, 1:1,000), LDHA (Cell Signaling Technology, cat. #2012, 1:1,000), phospho FOXO3a ser294 (Cell Signaling Technology, cat. #5538, 1:1,000), FOXO3a (Millipore, cat. #07-702), HA-Tag (Cell Signaling Technology, cat. #3724, 1:1,000), SOD2 (Cell Signaling Technology; cat. #13141, 1:1,000). Antibodies for IHC: PINK 1:100 (Sigma, HPA001931) and ki67 (Dako 1:100).

In vivo mouse model experiments

Mice were maintained in accordance with animal care practices at The Hospital for Sick Children, and approved following review of submitted protocol (0204-H). Stereotactic guided intracranial injections in NOD-SCID mice were performed as previously described (17). Flank injections were performed by injecting 2×10^6 million cells in 250 μL of PBS mixed with 250 μL of Matrigel (BD Biosciences, cat. #356234) into the flank of nude NOD-SCID mice. Mice were monitored for tumor growth, and tumor volumes were measured by a calliper.

Drosophila studies

All experimental fly crosses were maintained in circadian incubators (Darwin Chambers Company) at 25°C for egg-laying and larval development. Fly larval brains were dissected at wondering late third instar (96 hours after larval hatching) for tumor volume comparison and immunohistochemistry. Primary antibodies include: mouse-anti-Repo (Developmental Studies Hybridoma Bank, 1:10) and rabbit anti-phospho-Histone 3 (Millipore, 1:200). Fluorescence images and volumetric were carried out as previously described (18).

Other methods

Bromodeoxyuridine (BrdUrd) cell proliferation assay, caspase activity assays, colony-forming assays hexokinase activity, and PKM activity assays were performed as previously described (19).

Statistical analysis

All experiments were performed in triplicate with mean and SEM reported where appropriate. ANOVA was conducted for multigroup comparisons followed by a *post-hoc* Dunnett's test (groups compared with one control group) or *post-hoc* Tukey's test (to identify differences among subgroups). Where appropriate, direct comparisons were conducted using an unpaired two-tailed Student *t* test. Survival analysis was performed using the log-rank survival test. Significance was established (*, $P < 0.05$).

Results

Retroviral gene-trap and functional characterization of trapped clones

Primary astrocyte cultures were established from normal CD1-ICR (normal murine astrocytes, NMA), newborn hyperactivated Hras mice (B8-P0) mice and p53 null mice ($p53^{-/-}$). To identify loss of function events for transformation of early passage astrocytes, we transduced astrocytes with a retroviral gene trap vector (Fig. 1A and Supplementary Fig. S1A) containing a splice acceptor immediately upstream of a luciferase reporter gene with an IRES puromycin resistance marker. Using puromycin selection, we selected 32 resistant clones, 14 of which expressed luciferase (Supplementary Fig. S1B). Of the 14 luciferase-expressing gene-trap clones of varying backgrounds, 9 grew in soft agarose, a measure of transformation (Fig. 1B). NMAs were not transformed despite generating 5 puromycin resistant luciferase-expressing clones (Supplementary Fig. S1C). Inverse PCR identified gene insertion sites in 7 of the 9 anchorage-independent gene-trapped clones (Supplementary Table S1). GT-15 (Rap1Gap) and GT-16 (Ikkb) were previously reported in glioma biology (20, 21). Four of our genes identified have not been previously implicated in glioblastoma pathogenesis and were further characterized for cell growth, resistance to apoptosis, and invasion.

On the $p53^{-/-}$ background, we identified insertions in the following genes: GT-6 (Mitochondrial ribosomal protein S6/Mrsp6), and GT-8 (Storkhead box 1/Stox1). Compared with parental $p53^{-/-}$ cells, GT-8 but not GT-6 cells had increased proliferation as measured by BrdUrd proliferation assay over 7 days (Fig. 1C; *, $P < 0.05$). Both GT-6 and GT-8 demonstrated reduced caspase activity following exposure to 5 Gy irradiation or 1 μmol/L doxorubicin (common inducers of apoptosis) compared with parental $p53^{-/-}$ cells and non-modified murine astrocytes (Fig. 1D; *, $P < 0.05$). Both GT-6 and GT-8 had elevated

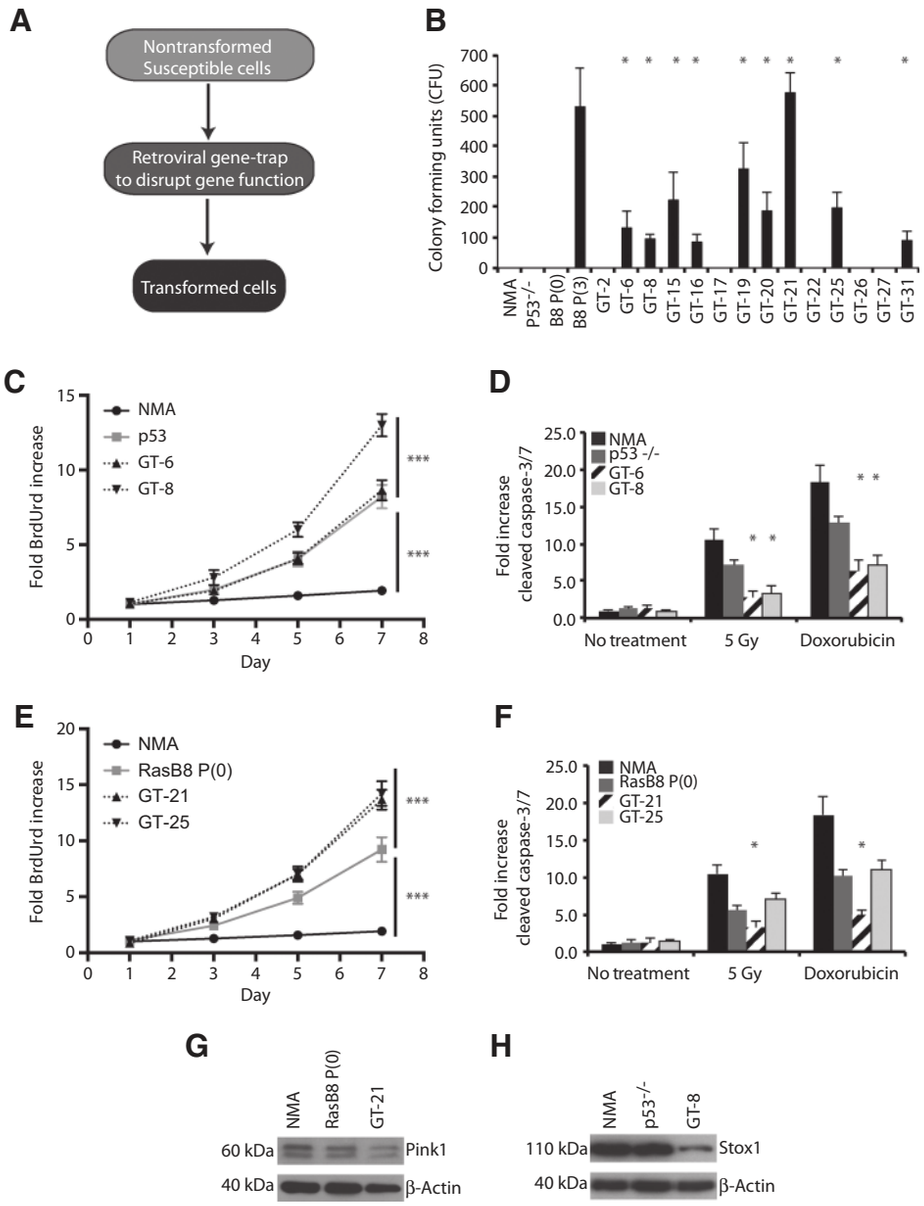

Figure 1.
Retroviral gene-trap and functional characterization of trapped clones. **A,** general strategy for retroviral gene-trap. **B,** trapped clones expressing luciferase had significant growth in soft-agar assays (9/14) compared with nontransformed astrocytes. Colony-forming units were counted on day 14 from seeding 5,000 cells. **C,** BrdUrd proliferation assay of gene-trapped clones from $p53^{-/-}$ background. **D,** activated cleaved caspase-3 and -7 Elisa assay on gene-trapped clones from $p53^{-/-}$ astrocytes. **E,** BrdUrd proliferation assay of gene-trapped clones from RasB8 background. **F,** activated cleaved caspase-3 and -7 Elisa assay on gene-trapped clones from RasB8 astrocytes. **G–H,** Western blot analysis demonstrating reduced Pink1 and Stox1 in trapped clones versus parental cells. The top band represents the full-length PINK1 and the bottom band represents a mature form of PINK1 that is cleaved following integration into the mitochondria. *, $P < 0.05$; ***, $P < 0.001$.

colony formation when treated with 5 Gy radiation compared with control cells (Supplementary Fig. S1D).

On the Ras-B8 P(0) background, we characterized GT-21 (PTEN-induced kinase 1/Pink1) and GT-25 (Suppressor of cytokine signaling 2/Socs2). GT-21 and GT-25 cells had increased proliferation as measured by BrdUrd incorporation over 7 days (Fig. 1E; *, $P < 0.05$) compared with controls. GT-21 and GT-25 showed reduced caspase activity following exposure to 5 Gy irradiation and treatment with doxorubicin compared with control cells (Fig. 1F; *, $P < 0.05$). GT-21 had elevated colony formation when treated with 5Gy radiation compared with control cells (Supplementary Fig. S1D) and GT-21 cells were the only cells with increased invasion compared with control cells (Supplementary Fig. S1F–S1G; *, $P < 0.05$). In summary, GT-21 had alterations in all four assays tested. Western blot analysis confirmed that these gene-trap events altered protein expression of our two top candidates: PINK1 and STOX1 (Fig. 1G and H).

Loss of PINK1 alters normal human astrocyte metabolism

To investigate the role of our top candidate, PINK1, with respect to cell growth, oxidative stress, and mitochondrial function in human cell systems, we performed functional validation in normal fetal human astrocytes (NHA) and several established human glioblastoma cells. PINK1 expression was detected in primary cultures of human fetal astrocytes, but low or negative in most glioblastoma cell lines and explant cultures (GBM8 and GBM12; Fig. 2A and B). Cellular fractionation analysis demonstrated that PINK1 was predominantly localized to the mitochondria (Supplementary Fig. S2A). Because the impact of PINK1 loss on normal human astrocytes is poorly characterized, we generated stable PINK1 knockdown clones mediated by two pooled shRNA

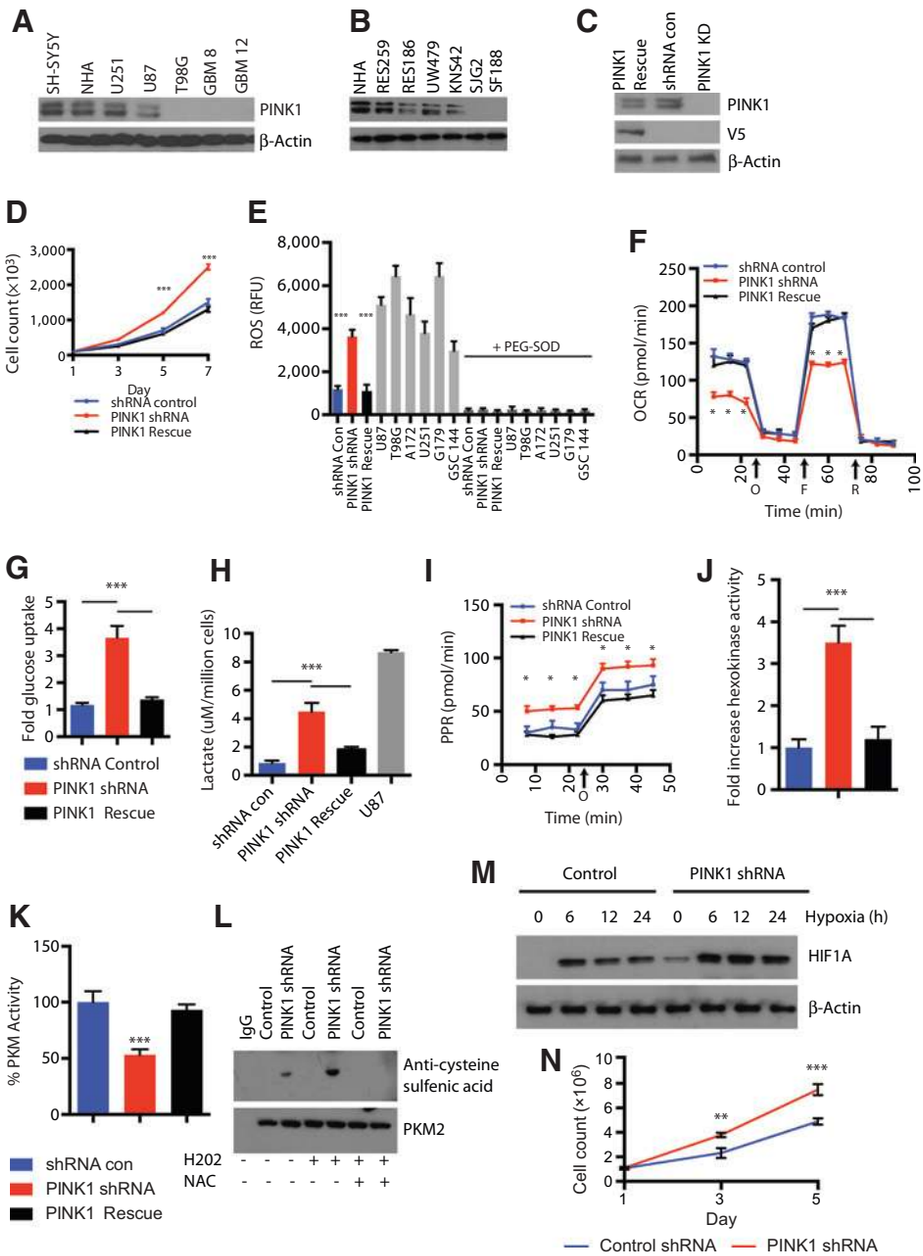

Figure 2.

Loss of PINK1 alters normal astrocyte metabolism. **A,** Western blot analysis demonstrating variable expression of PINK1 in NHAs, glioblastoma cell lines, and glioblastoma explants (GBM8 and GBM12). **B,** Western blot analysis of PINK1 in pediatric glioblastoma cell lines. **C,** Western blot analysis of PINK1 pooled stable shRNA knockdown in NHAs, shRNA control NHAs and V5-tagged PINK1 rescue NHAs. **D,** cell count assay of PINK1 shRNA NHAs compared with control shRNA NHAs. **E,** NHA control shRNA, NHA PINK1 KD cells and glioblastoma cells were assayed for endogenous ROS. Measurements were obtained using an ROS-sensitive probe (1 μmol/L chloromethyl-H2DCFDA). Fluorescence ROS signal was quenched with addition of 100 μ/mL PEG-SOD. **F,** OCR of NHAs compared with NHAs with PINK1 knockdown after exposure to varying bioenergetic modulators: oligomycin (O), carbonyl cyanide 4-(trifluoromethoxy) phenylhydrazone (FCCP/F), and rotenone (R). Arrow denotes when compounds were added. **G,** glucose uptake in cells measured by incubation with the fluorescent glucose analogue 2-NBDG. U87 cells were used as a positive control. **H,** extracellular lactate in cells described in **D** was measured by a NADH-coupled enzyme reaction with absorbance measured at 490 nm on day 3 and normalized to cell number. U87 cells were used as a positive control. **I,** glycolytic flux analysis measurement. Proton production rate (PPR, pmol/min) was measured in U87 empty vector control cells compared to U87 PINK1–overexpressing cells. Arrow with O represents addition of oligomycin to inhibit ATP synthase and measure maximum glycolytic capacity of cells. **J,** fold increase of total HK activity normalized to scrambled shRNA in cells. **K,** pyruvate kinase activity assay of control shRNA NHAs versus PINK1 shRNA NHAs. PKM activity assay was performed on day 3 and normalized to 10 μg of cell lysate. **L,** immunoprecipitation of PKM2 in 1% SDS was analyzed by standard Western and blotted with an anti-cysteine sulfenic acid antibody demonstrating oxidized cysteine residues on PKM2 in the presence or absence of H_2O_2 (1 mmol/L) and oxidizing agent and N-acetyl cysteine (NAC, 5 mmol/L). **M,** Western blot demonstrating HIF1A stabilization in control and PINK1 knockdown cells exposed to normoxia and varying time points of hypoxia (1% O_2). **N,** cell count assay of PINK1 shRNA NHAs compared with control shRNA NHAs in 1% hypoxia. *, $P < 0.05$; **, $P < 0.01$; ***, $P < 0.001$.

constructs targeting PINK1 as well as a PINK1 rescue line where a V5 epitope–tagged PINK1 was re-introduced into knockdown cells (Fig. 2C). Knockdown of PINK1 led to increased proliferation as measured by cell count over 7 days compared with scrambled control and PINK1 rescue cells (Fig. 2D; *, $P < 0.05$). We observed no change in mitochondrial copy number or cell size in PINK1 knockdown and control cells (Supplementary Fig. S2B and S2C). We next measured oxidative stress and ROS using a cell permeable fluorescent probe (2′-7′ Dichlorodihydrofluorescein diacetate; DCFH-DA). PINK1 knockdown cells had elevated endogenous ROS levels that were comparable with glioblastoma cells whereas control and PINK1 rescue cells had significantly lower amounts of ROS (Fig. 2E; *, $P < 0.05$). To ascribe the changes of probe oxidation to ROS, fluorescence signal was blocked when the experiment was repeated with addition of 100 U/mL PEG-SOD (Fig. 2E; *, $P < 0.05$). As an added control for fluorescence signal, we repeated the experiment with an oxidation insensitive analog probe [carboxy-DCFDA (5-(and-6)-carboxy-2',7'-dichlorofluorescein diacetate] and observed no changes in fluorescence between groups (Supplementary Fig. S2D), supporting our DCFH2-based ROS measurements were due to probe oxidation. Treatment of PINK1 knockdown cells with mito-TEMPO, a mitochondrial antioxidant suppressed ROS but not when cells were treated with a NADPH oxidase inhibitor (diphenyleneiodonium), supporting PINK1 suppressed mitochondrial ROS (Supplementary Fig. S2E). Overexpression of HA-tagged mitochondrial superoxide dismutase 2 (SOD2) in PINK knockdown cells suppressed ROS and fully rescued several phenotypes induced by PINK1 knockdown namely cell growth, glucose uptake, lactate, hexokinase, and pyruvate kinase activity (Supplementary Fig. S2F–S2M).

Loss of PINK1 resulted in a significantly reduced basal oxygen consumption rate (OCR) and significantly reduced maximum OCR when stimulated with a mitochondrial oxidative phosphorylation (oxphos) decoupling agent FCCP (Carbonyl cyanide 4-(trifluoromethoxy) phenylhydrazone; Fig. 2F; *, $P < 0.05$). PINK1 knockdown cells also exhibited increased glucose uptake and lactate compared with control and PINK1 rescue cells (Fig. 2G and H; *, $P < 0.05$). PINK1 knockdown cells also had increased basal glycolysis and higher maximum glycolytic capacity when treated with treated with oligomycin (an ATP synthase inhibitor used to measure ATP coupled oxphos) compared with controls (Fig. 2I; *, $P < 0.05$). Increased hexokinase activity (Fig. 2J; *, $P < 0.05$) and increased expression of several glycolytic genes (Supplementary Fig. S3A) were observed in knockdown but not control cells.

PINK1 loss promotes inactivation of PKM2 and stabilizes HIF1A

Pyruvate kinase M2 isoform (PKM2), HIF1A and its target genes are known to be essential for aerobic glycolysis. Several studies have demonstrated that cancer cells have elevated glycolysis and reduced PKM2 activity, which is associated with increased lactate compared with nontransformed cells (22). One mechanism of PKM2 reduced activity observed in highly glycolytic cells is mediated by ROS (22, 23). PINK1 knockdown cells had reduced total pyruvate kinase (PKM) activity compared with control and rescue cells (Fig. 2K; *, $P < 0.05$). Our NHA cells expressed the PKM2 and not PKM1 making our assay specific to PKM2 activity (Supplementary Fig. S3B).

ROS are negative regulators of PKM2, which oxidize cysteine residues on PKM2 preventing tetramerization required for efficient activity (23) and hypothesized that elevated ROS in PINK1 knockdown cells may reduce PKM2 activity through oxidization cysteine amino acids. We detected oxidized cysteine amino acids in PKM2 immunoprecipitates from PINK1 knockdown cells but not controls (Fig. 2L). Treatment with hydrogen peroxide, a form of intracellular ROS, further increased the level of oxidized cysteine in PKM2 (Fig. 2L). This increase was abolished by the addition of N-acetyl cysteine (NAC), a strong reducing agent (Fig. 2L). Elevated ROS levels have also been shown to increase and stabilize HIF1A signaling (24, 25). We also observed increased HIF1A protein levels under normoxic conditions in PINK1 knockdown NHAs but not control cells (Fig. 2M). PINK1 knockdown cells treated with 1% hypoxia maintained significantly increased HIF1A protein levels across several time points and an increase in proliferation during hypoxia (Fig. 2M and N and Supplementary Fig. S3C; *, $P < 0.05$). As validation, HIF1A targets, which regulate the shift to glycolytic metabolism, LDHA, PDK1 and PKM2, were up-regulated in PINK1 knockdown cells (Supplementary Fig. S3D; *, $P < 0.05$). Cell proliferation and invasion was partially rescued when PINK1 knockdown cells were treated with HIF1A siRNA under normoxia and hypoxia (Supplementary Fig. S3E–S3H). PINK1 knockdown cells treated with NAC had decreased HIF1A levels under normoxia and hypoxia conditions, resulting in reduced ROS and increased cell-doubling time (Supplementary Fig. S4A–S4C; *, $P < 0.05$).

PINK1 overexpression stops glioblastoma cell growth and reduces ROS

To complement our knockdown experiment, we next explored the effect of PINK1 stable expression in U87, T98G, and SF188 cells. We generated pooled stable PINK1-V5 epitope tagged and empty vector control cell lines. Expression of PINK1 significantly reduced cell proliferation over a period of 7 days in all three cell lines and cell invasion (Fig. 3A and B and Supplementary Fig. S5A) with PINK1 stable expression confirmed by Western blot analysis (Fig. 3C). PINK1 expression reduced basal HIF1A in normoxia and reduced aerobic glycolysis and HIF1A response proteins: PDK1, HK2, LDHA, and VEGFA (Fig. 3C). Pyruvate dehydrogenase kinase 1, PDK1, an HIF1A target inhibits pyruvate entry into the citric acid cycle by phosphorylating pyruvate dehydrogenase E1 alpha (PDHE1a) a mitochondrial protein responsible for decarboxylation of pyruvate into acetyl-CoA. We observed that reduced PDK1 in PINK1-overexpressing cells led to reduced phospho-PDHE1a, supporting that the inhibitory effect of PDK1 on PDHE1a was diminished (Fig. 3C). PINK1-expressing cell lines also had significant reduction in ROS (Fig. 3D and Supplementary Fig. S5B; *, $P < 0.05$), reduced cell growth in hypoxia (Fig. 3E; *, $P < 0.05$) and reduced HIF1A protein expression in hypoxia compared to empty vector control cells (Fig. 3F). PDK1, an HIF1A target gene critical in the HIF1A response to hypoxia, was also downregulated confirming reduced activity of the HIF1A in hypoxia (Fig. 3F).

PINK1 inhibits aerobic glycolysis in glioblastoma cells

In contrast to PINK1 knock down, U87 cells stably expressing PINK1 had a significant increase in basal OCR, increased maximum OCR when treated with FCCP, reduced basal glycolytic and max glycolytic capacity flux as measured proton production rate

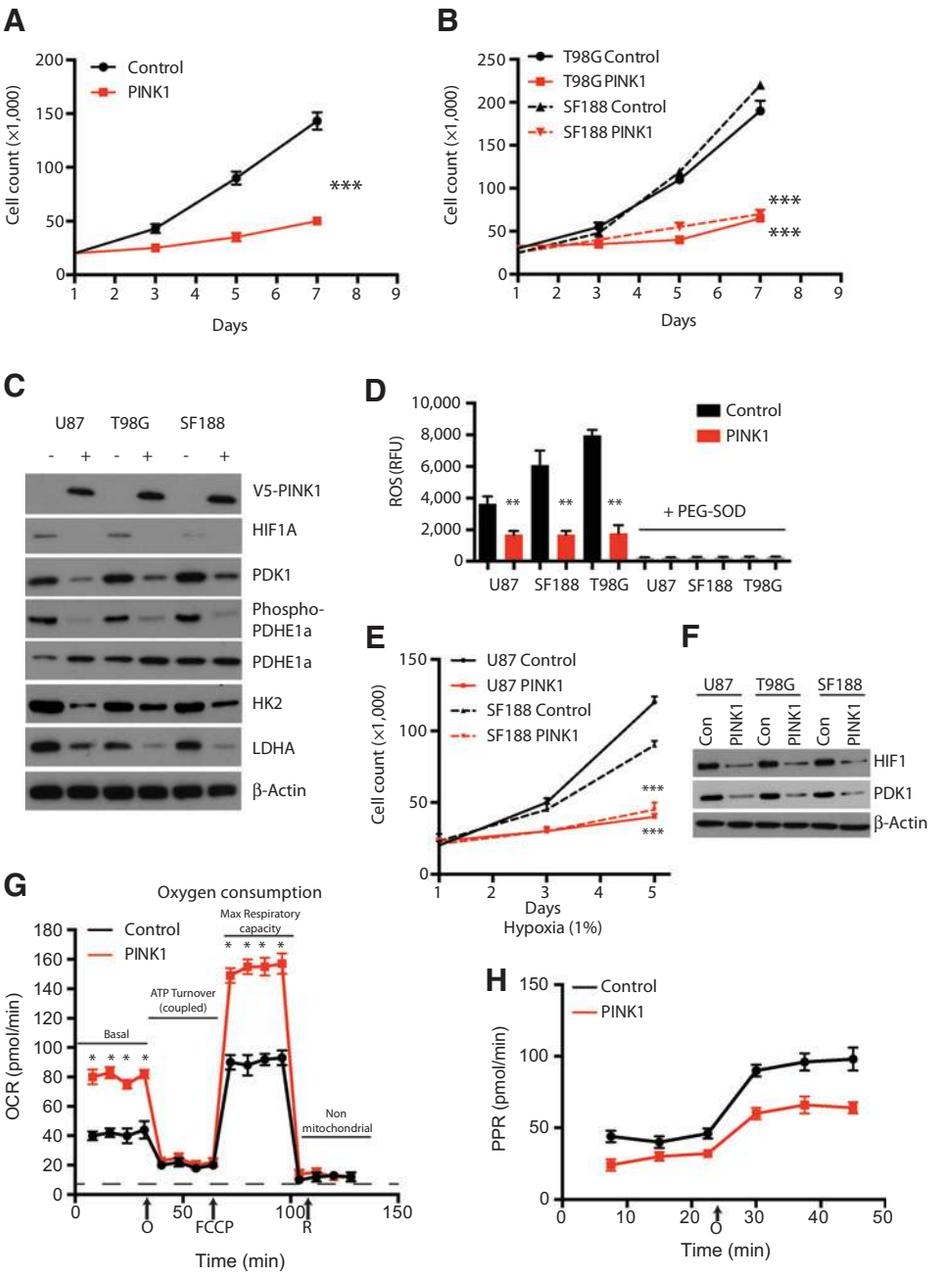

Figure 3.

PINK1 overexpression stops glioblastoma cell growth and inhibits glycolysis proteins. **A,** proliferation assay of U87 empty vector control cells compared with U87 PINK1-overexpressing cells over 7 days. **B,** proliferation assay of SF188 and T98G empty vector control cells compared with SF188 or T98G PINK1–overexpressing cells over 7 days. **C,** Western blot analysis confirming stable expression of V5-tagged PINK1 protein and several proteins involved in glycolysis and HIF1A targets. **D,** ROS measurements of glioblastoma cells expressing empty vector controls or PINK1 stable expression. Fluorescence ROS signal was quenched with addition of 100 μ/mL PEG-SOD. **E,** cell growth assay of SF188 and U87 empty vector control cells compared with SF188 or U87 PINK1–overexpressing cells over 5 days in hypoxia (1% O_2). **F,** Western blot analysis assaying for HIF1A and an HIF1A target gene PDK1 in hypoxia (1% O_2) at 72 hours in empty vector control or PINK1 stable–expressing cells. **G,** OCRs of U87 empty vector control cells compared to U87 PINK1–overexpressing cells varying bioenergetic modulators: Oligomycin (O), carbonyl cyanide 4-(trifluoromethoxy) phenylhydrazone (FCCP/F), and rotenone (R). Arrow denotes when compounds were added. **H,** glycolytic flux analysis measuring proton production rate (PPR, pmol/min). Arrow with O represents addition of oligomycin to inhibit ATP synthase and measure maximum glycolytic capacity of cells. *, $P < 0.05$; **, $P < 0.01$; ***, $P < 0.001$.

(PPR) compared to control cells (Fig. 3G and H; *, $P < 0.05$). T98G and SF188 PINK1 stably expressing cells also had increased oxygen consumption (Supplementary Fig. S5C and S5D). All glioblastoma cells had reduced hexokinase activity, increased PKM activity (Supplementary Fig. S5E–S5F; *, $P < 0.05$). U87, SF188 and T98G stably expressing PINK1 had reduced glucose uptake and reduced lactate measured over several days (Supplementary Fig. S6A–S6F; *, $P < 0.05$) compared with controls.

We next expressed PINK1 in primary glioblastoma cultures that were serially passaged in mice to better maintain molecular features of glioblastoma (26, 27). PINK1 expression in GBM8 and GBM12 explant cultures reduced cell growth, invasion, glucose uptake, lactate and hexokinase activity (Supplementary Fig. S7A–S7F; *, $P < 0.05$). FOXO transcription factor activation, including FOXO3a, has been shown to inhibit ROS and HIF1A stabilization (28, 29). We hypothesized that PINK1 expression may result in FOXO3a activation. Both U87 and T98G control cells express inhibitory phosphorylation of FOXO3a at serine residue 294 (Fig. 4A). PINK1-expressing U87 and T98G cells had reduction of this inhibitory phosphorylation site and increased SOD2, a target of FOXO3a and increased SOD activity (Fig. 4A and Supplementary Fig. S7G) supporting that PINK1 inhibited ROS signaling. Loss of FOXO3a by pooled siRNA rescued ROS production inhibited by PINK1 and we repeated the experiment with the addition of PEG-SOD to ascribe the changes in probe oxidation to ROS (Fig. 4B). FOXO3a knockdown also rescued the

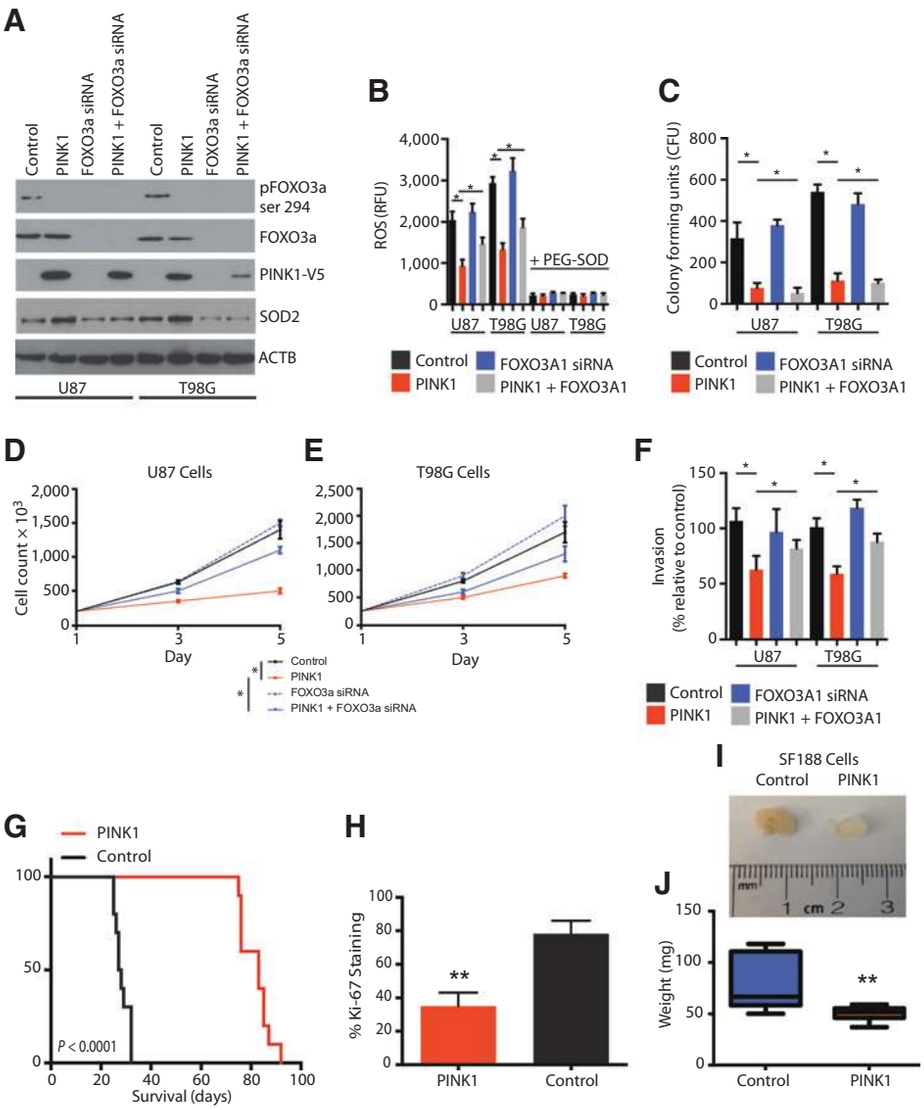

Figure 4.
PINK1 inhibits aerobic glycolysis in glioblastoma cells. **A,** Western blot analysis of U87 and T98G cells after FOXO3a pooled siRNA treatment and control siRNA-treated cells. **B,** ROS measurement measured at 48 hours from cells expressing control vector or PINK1 treated with FOXO3a siRNA. Fluorescence ROS signal was quenched with addition of 100 μ/mL PEG-SOD. **C,** colony-forming assay cells: 500 cells were plated in 6-well plates. Colonies were scored on day 10. **D,** cell counts of U87 cells with control vector, PINK1 and FOXO3a siRNA. **E,** cell counts of T98G cells with control vector, PINK1, and FOXO3a siRNA. **F,** invasion assay of control cells, PINK1-expressing cells, and FOXO3a at 12 hours. **G,** Kaplan–Meier survival curve analysis of an orthotopic xenograft model of glioblastoma. U87 ($n = 10$) empty vector control or PINK1-expressing cells ($n = 10$). **H,** quantification of Ki-67 from Fig. 4G. Ki-67 was analyzed by quantification of 20 fields of view and 5 mice per condition. **I,** image of tumor xenografts removed from SF188 control cells and SF188 PINK1-overexpressing cells after 14 days flank implantation in NOD-SCID mice. **J,** quantification of weight of tumors from **I** after 14 days flank implantation in NOD-SCID mice. *, $P < 0.05$; **, $P < 0.01$.

anticolony forming ability, anti-cell proliferation, and reduced invasion phenotypes caused by PINK1 expression (Fig. 4C–F; *, $P < 0.05$).

Selective targeting in PINK1-expressing glioblastoma cells leads to reduced viability

We observed PINK1 expression in some glioblastoma cell lines (U118 and U251) and two GBM cancer stem cell lines (G179 and G144). We postulated that PINK1 loss this context would elevate ROS levels to a growth-inhibiting level, as ROS can also promote anti-growth affects. We used pooled siRNA-mediated silencing of PINK1 in glioblastoma cancer stem cell enriched cultures G179 and G144 and glioblastoma cell lines U118 and U251. Loss of PINK1 resulted in reduced cell viability (Supplementary Fig. S8A–S8E; *, $P < 0.05$). PINK1 loss also resulted in further increased ROS levels compared with controls cells as measured with a DCFH-DA probe but not oxidation insensitive probe (Supplementary Fig. S8F and S8G; *, $P < 0.05$). Loss of PINK1 in glioblastoma cells led to increased and oxidative stress indicated by increases in $NADP^+$/NADPH ratios, and depletion of glutathione indicated by increased GSSG levels and decreased GSH:GSSG ratios compared with controls (Supplementary Fig. S6H–S6J). Oxidative stress can sensitize glioblastoma cells to cell death by ROS inducing treatments including radiation. PINK1 loss sensitized glioblastoma cells to apoptosis and reduced colony formation following treatment with 2 Gy irradiation (Supplementary Fig. S9A–S9H).

PINK1 suppresses glioblastoma growth *in vivo*

Using an orthotopic xenograft model, U87 control, or PINK1-overexpressing U87 cells were injected into the frontal cortex of immune-compromised mice. Compared with controls, mice bearing tumors with PINK1 overexpression had an approximate tripling median survival time (Fig. 4G, *, $P < 0.05$ and Supplementary Fig. S10A).

PINK1-expressing tumor cells also had significantly reduced in proliferation quantified by Ki-67 staining (Fig. 4H and Supplementary Fig. S10A). To evaluate the effect of PINK1 overexpression on tumor burden, we used a subcutaneous xenograft model of SF188 cells expressing PINK1. Average tumor weight of SF188 cells overexpressing PINK1 was significantly reduced by 50%

compared with control SF188 cells in the flank after 14 days of growth (Fig. 3I–J).

PINK1 expression in tumor models is evolutionarily conserved across highly distant species and to determine its role in the pathogenesis of EGFR/PI3K-activated glioblastomas, we generated a spontaneous *Drosophila* model of glioblastoma by overexpressing the fly orthologs of constitutively active EGFR ($dEGFR^{\lambda}$) and PI3K ($Dp110^{CAAX}$) in the glial cell lineage using the repo-Gal4 driver. Coactivation of EGFR-ras and PI3K signaling has been shown to promote glial proliferation and invasion, common features of human glioblastoma (Fig. 5A; ref. 30). In agreement with our findings in mammalian cells, we found that glial-specific overexpression of PINK1 significantly reduced the overall tumor volume compared to control tumors overexpressing mCherry (Fig. 5A and B). Our immunohistochemistry analyses revealed that PINK1-overexpressing tumors exhibited a marked reduction in the number of repo-positive glial cells, normally enriched in the periphery of brain lobes, compared with controls (Fig. 5C). Consistent with this robust phenotype, PINK1 overexpression resulted in pronounced proliferation defects as evidenced by decreased phospho-histone 3–positive mitotic cells compared with the mCherry-expressing controls (Fig. 5D). These findings highlight the evolutionarily conserved antitumor effect of PINK1 across distant species and suggest that its loss may be critical for the development of glioblastomas driven by mutational activation of growth factor receptor signaling pathways.

PINK1 is downregulated in brain tumors

Compared with normal brain, expression of *PINK1* mRNA in grade 2–3 gliomas was reduced with further reduction in glioblastoma (grade 4; Fig. 6A; *, $P < 0.05$) in the REMBRANDT dataset (31). PINK1 is located on chromosome 1p36, which is frequently deleted in low-grade gliomas. We detected PINK1 heterozygous loss in 103/285 (36%) low-grade samples and significantly lower PINK1 expression in low-grade gliomas with copy-number loss of PINK1 (Supplementary Fig. S10B; *, $P < 0.05$) in the TCGA low-grade glioma dataset (32). GBM transcriptional profiling studies have revealed that the disease comprises several molecular

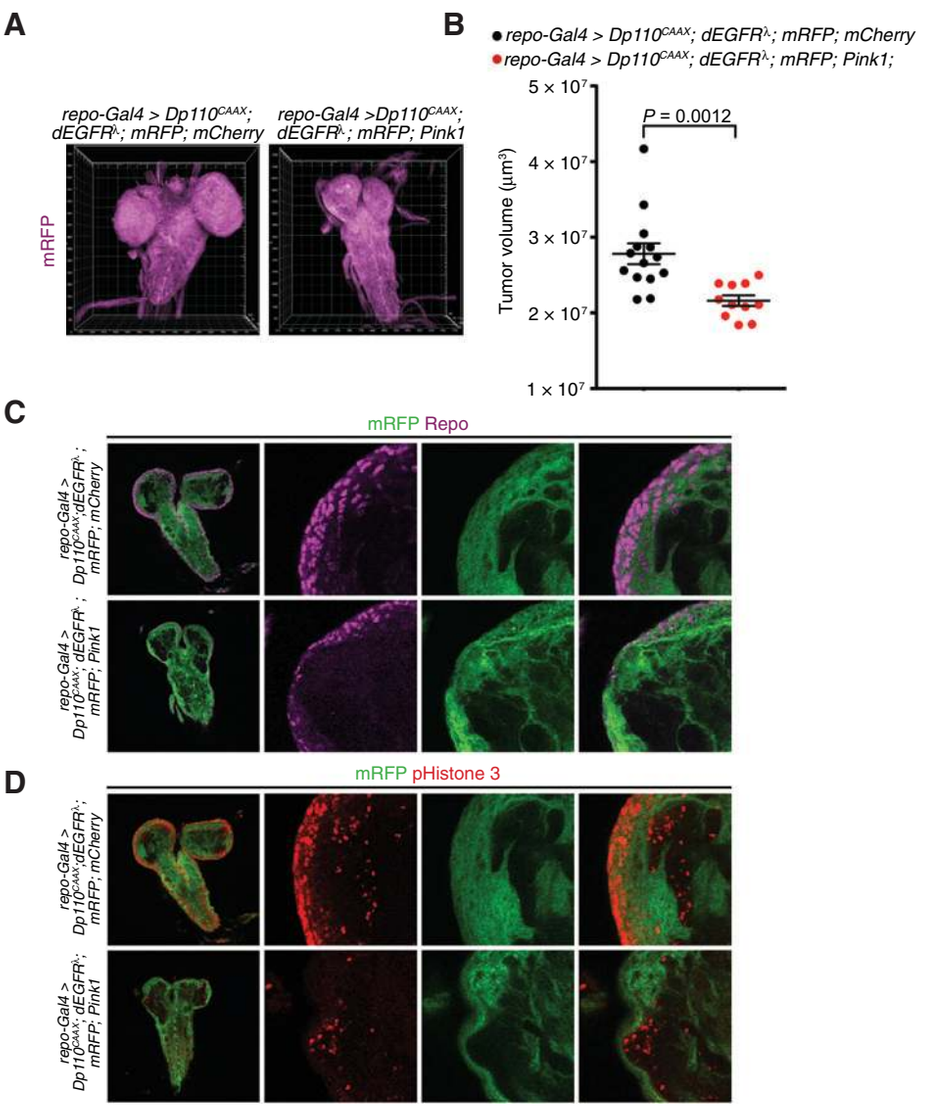

Figure 5.
Pink1 inhibits growth in a *Drosophila* model of glioblastoma. **A,** representative 3-D stacked confocal images of the glial tissue, marked by *repo-Gal4*–driven mRFP expression, in third instar larvae of the indicated genotypes. Note that Pink1 overexpression under the same driver induced marked reduction of overall glial tumor size. **B,** volume quantification shows significant decrease in size of the glial tumors with Pink1 overexpression compared with the control tumors expressing mCherry. **C,** representative single-optical slice (5 µmol/L) confocal images show marked reduction of the number of tumor cells labeled by the nuclear glial marker Repo and *repo-Gal4*–driven mRFP expression. **D,** representative single-optical slice (5 µmol/L) confocal images show reduction of the number of mitotic tumor cells labeled by the mitosis marker phospho-Histone 3 and *repo-Gal4*–driven mRFP expression.

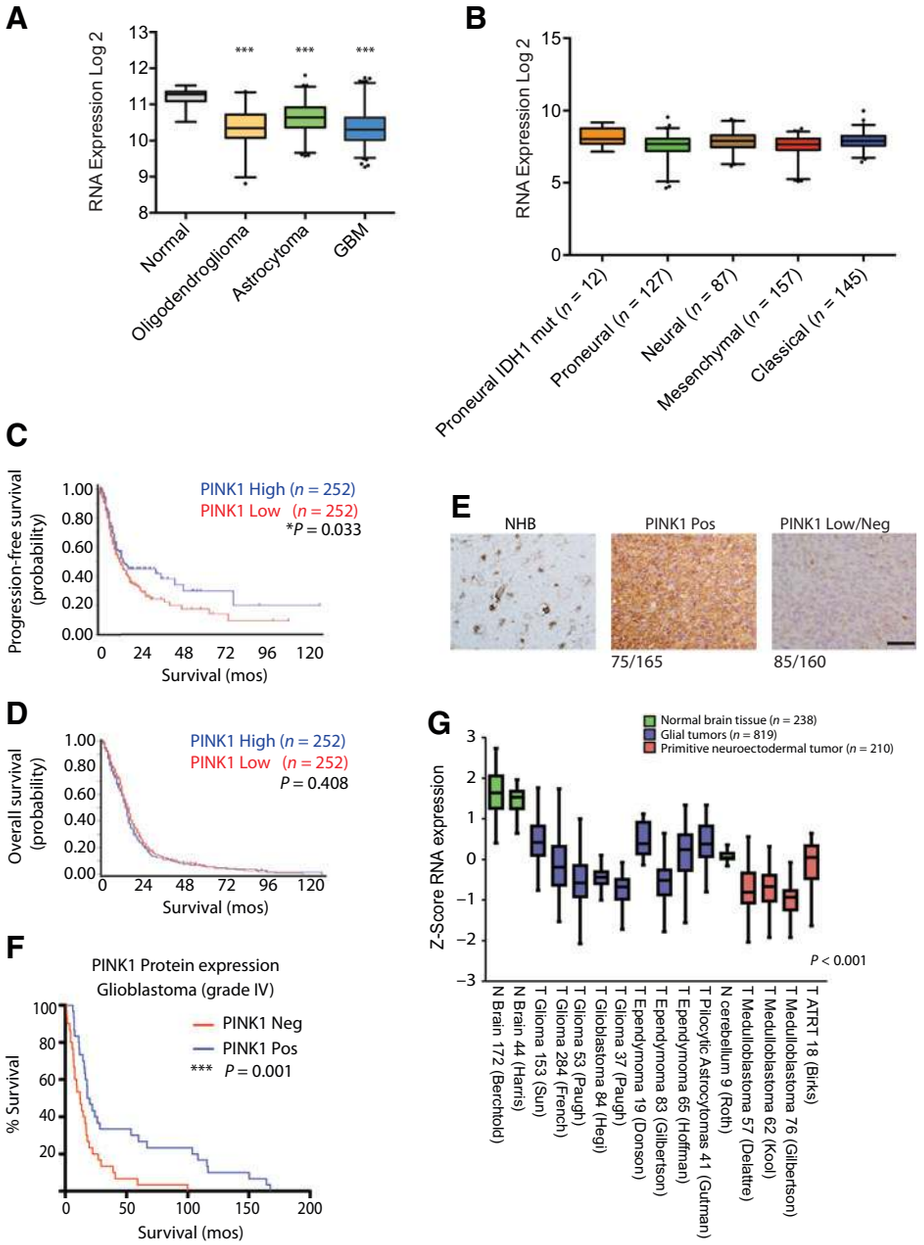

Figure 6.
PINK1 is downregulated in brain tumors. **A,** PINK1 gene expression in several glioma tumors compared with normal brain in the REMBRANDT dataset. **B,** PINK1 gene expression among varying glioblastoma subtypes from the TCGA dataset ($n = 528$). **C,** PINK1 high gene expression based on median RNA cutoff value correlated with increased PFS in the TCGA dataset. **D,** PINK1 high gene expression based on median RNA cutoff value is not associated with OS in the TCGA dataset. **E,** IHC analysis of PINK1 in normal brain and 160 glioblastoma-operative samples; scale bar, 50 μm. **F,** PINK1 survival analysis from a TMA of 61 glioblastoma patients given temozolomide and radiation. **G,** meta-analysis performed in R2 genomics software comparing normal brain of different regions (cortex for gliomas, cerebellum to over 900 primary brain tumors from 17 datasets and studies). PINK1 RNA expression was significantly downregulated in all datasets analyzed. ***, $P < 0.001$.

subtypes, each with unique genomic alterations and clinical behaviors (4, 27, 33). *PINK1* expression did not vary significantly across glioblastoma subtypes in the TCGA dataset (Fig. 6B; *, $P < 0.05$; ref. 4). At the RNA level, PINK1 expression correlated with significantly increased progression-free survival (PFS) but not overall survival (OS; Fig. 6C and D). Because of the dynamic regulation of PINK1 protein stability, transcriptional level analysis of PINK1 must be complemented with PINK1 protein level expression analysis (34). To address this, we performed IHC of over 160 glioblastoma tumor tissue samples and detected PINK1 loss in 53% of glioblastoma samples (85/160; Fig. 6E). Tissue microarray analysis (TMA) of primary glioblastoma tumors previously treated with concomitant temozolomide and radiation therapies revealed a correlation between PINK1 negative tumors and worse OS (Fig. 6F; *, $P < 0.05$).

Gene-expression analysis of 238 normal brain tissue samples and 984 primary brain tumors was next performed to determine with PINK1 loss is observed in other brain tumors. Compared with location matched normal brain, PINK1 was significantly downregulated in several primary brain tumors including glioblastoma (Fig. 6G). PINK1 loss was also observed in all four molecular subgroups of medulloblastoma; a common brain tumor in children (Supplementary Fig. S10C).

Discussion

Metabolic reprogramming is essential for cancer cells to generate biomass and reducing power in the form of NADPH and GSH to fuel these biosynthetic pathways and buffer against ROS-induced. We demonstrate that PINK1 is a driver in

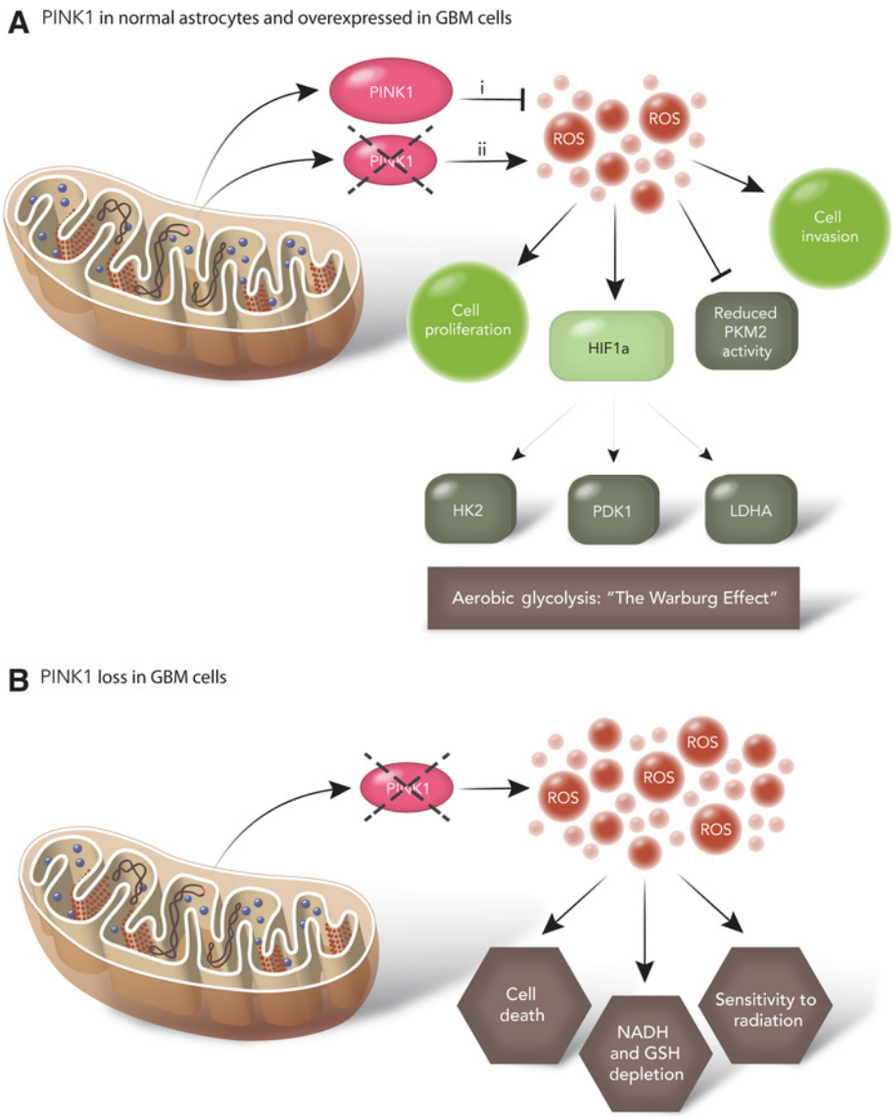

Figure 7.
Summary of PINK1 function in glioma. **A, i,** PINK1 in normal astrocytes or when re-expressed in glioblastoma cells suppresses ROS and inhibits aerobic glycolysis. **ii,** loss of PINK1 in normal astrocytes increases ROS, stabilizing HIF1α and promoting the Warburg effect/aerobic glycolysis. **B,** loss of PINK1 in glioblastoma cells increases ROS to high levels, triggering oxidative stress that triggers cell death, depletion of antioxidant molecules, and sensitizes cells to radiation.

glioblastoma biology as its loss leads to in increased proliferation, reduced oxygen consumption, and increased glycolysis, as measured by lactate production and glucose uptake. Our data support that re-expression of PINK1 can suppress growth in glioblastoma cells both *in vivo* and *in vitro*. Reduction in PINK1 expression caused HIF1A stabilization via elevation of ROS. Cancer cells increase aerobic glycolysis through the Warburg effect and produce higher levels of oxidative stress via ROS (14, 35). ROS generation, accumulation, and elimination must be tightly regulated in cancer cells to prevent cell death. Imbalances in ROS generation and elimination can alter cell phenotypes in both normal and tumor cells. Loss of PINK1 in NHAs increases ROS levels and promotes aerobic glycolysis via stabilization of HIF1A (36). Loss of PINK1 has been shown to stabilize HIF1A in murine neurons and murine fibroblasts to sustain proliferation (37). Pink1 loss in zebrafish has been shown to activate HIF1A target genes; however, HIF1A protein expression and the effect on aerobic glycolysis were not assessed (38). In murine astrocytes (NMA), Pink1 loss has been shown to increase glucose metabolism through stabilization of HIF1A in murine astrocytes (NMAs; ref. 37). Our study sheds new light on how Pink1 regulates HIF1A levels in cancer cells, promoting glucose uptake and utilization to drive tumor growth.

PINK1 overexpression in glioblastoma cells reduces ROS production and may inhibit ROS-driven phenotypes including aerobic glycolysis and proliferation (Fig. 7A). These results are consistent with previous studies demonstrating that lower levels of ROS scavenging enzymes, including SIRT3, can promote aerobic glycolysis and metabolic reprogramming in both normal and cancer cells while overexpression reduces cancer cell growth (36, 39, 40). We observed that PINK1 overexpression inhibited ROS and metabolic reprogramming through FOXO3a, a master regulator of antioxidant pathways. PINK1 and FOXO3a have been shown to work cooperatively in noncancer cells (41, 42). Furthermore, overexpression of mitochondrial superoxide dismutate 2 SOD2 in our study can rescue several the phenotypes observed with loss of PINK1, a downstream target of FOXO3a and has been shown to be a tumor suppressor in cancer cells (43).

Not all cell types respond to PINK1 loss in the same manner as PINK1 loss results in variable responses in different cell types and

contexts (44). Loss of PINK1 expression in neurons and several other cell types has been shown to induce cell death (10, 11, 45). One study observed that *Pink1*$^{-/-}$ mouse astrocytes proliferate slower than control astrocytes (46). We observed PINK1 downregulation increased cell proliferation and this difference could be attributed to the fact that we were unable to completely abolish PINK1 expression and maintained a progrowth threshold of ROS.

ROS has both pro- and antigrowth affects in cancer cells (14, 47). Although we report that ROS activation via PINK1 loss in astrocytes acts as a pro-growth signaling response, it is conceivable that increased ROS could have detrimental effects on cancer cells as summarized in Fig. 7B. This is supported by our observation that PINK1 loss in certain glioblastoma cells results in excessive ROS generation and cell death and another study where PINK1 inhibition in mismatch repair deficient cancer cells results in an elevation of ROS and cell death (48). Furthermore, the identification of PINK1 in our screen was in astrocytes harboring activated Ras and the interplay of PINK1 and Ras signaling on metabolism and ROS still remains to be elucidated.

PINK1 is located on chromosome 1p36, a recurrent deleted hotspot in several cancers (32, 49). We detected loss of PINK1 at the DNA, RNA, protein level, and observed PINK1 protein–expressing glioblastoma patients had better survival. We did not detect copy-number gains or RNA overexpression, suggesting a role against PINK1 serving as an oncogene. Evidence also supports the role of PINK1 as a tumor-suppressor gene in ovarian and breast cancer (50, 51).

Identification of PINK1 substrates or therapeutic compounds that exploit ROS may be efficacious in treating glioblastomas and other cancers.

Disclosure of Potential Conflicts of Interest

No potential conflicts of interest were disclosed.

Authors' Contributions

Conception and design: S. Agnihotri, B. Golbourn, M.D. Taylor, G. Zadeh, J.T. Rutka

Development of methodology: S. Agnihotri, B. Golbourn, D. Mackenzie, G. Zadeh

Acquisition of data (provided animals, acquired and managed patients, provided facilities, etc.): S. Agnihotri, B. Golbourn, X. Huang, S. Younger, R.A. Cairns, A. Chalil, D. Mackenzie, V. Ramaswamy, M.S. Taccone, G.N. Fuller

Analysis and interpretation of data (e.g., statistical analysis, biostatistics, computational analysis): S. Agnihotri, B. Golbourn, X. Huang, M. Remke, R.A. Cairns, A. Chalil, V. Ramaswamy, P.S. Mischel, M.D. Taylor, J.T. Rutka

Writing, review, and/or revision of the manuscript: S. Agnihotri, B. Golbourn, M. Remke, P. Rakopoulos, P.S. Mischel, G.N. Fuller, C. Hawkins, W.L. Stanford, M.D. Taylor, G. Zadeh, J.T. Rutka

Administrative, technical, or material support (i.e., reporting or organizing data, constructing databases): S. Agnihotri, S. Younger, C.A Smith, M.S. Taccone, P.S. Mischel

Study supervision: S. Agnihotri, C.A Smith, C. Hawkins, G. Zadeh, J.T. Rutka

Other (created the figures to accompany the data): S.-L. Krumholtz

Grant Support

This study was funded by Canadian Institutes of Health Research grants (CIHR MOP-76410), Brainchild, and the Laurie Berman and Wiley Family Funds for Brain Tumor Research (J.T. Rutka).

The costs of publication of this article were defrayed in part by the payment of page charges. This article must therefore be hereby marked *advertisement* in accordance with 18 U.S.C. Section 1734 solely to indicate this fact.

Received November 16, 2015; revised May 8, 2016; accepted June 2, 2016; published OnlineFirst June 20, 2016.

References

1. Hegi ME, Diserens AC, Gorlia T, Hamou MF, de Tribolet N, Weller M, et al. MGMT gene silencing and benefit from temozolomide in glioblastoma. N Engl J Med 2005;352:997–1003.
2. Stupp R, Hegi ME, Mason WP, van den Bent MJ, Taphoorn MJ, Janzer RC, et al. Effects of radiotherapy with concomitant and adjuvant temozolomide versus radiotherapy alone on survival in glioblastoma in a randomised phase III study: 5-year analysis of the EORTC-NCIC trial. Lancet Oncol 2009;10:459–66.
3. Ding H, Roncari L, Shannon P, Wu X, Lau N, Karaskova J, et al. Astrocyte-specific expression of activated p21-ras results in malignant astrocytoma formation in a transgenic mouse model of human gliomas. Cancer Res 2001;61:3826–36.
4. Brennan CW, Verhaak RG, McKenna A, Campos B, Noushmehr H, Salama SR, et al. The somatic genomic landscape of glioblastoma. Cell 2013;155:462–77.
5. Network TCG.Comprehensive genomic characterization defines human glioblastoma genes and core pathways. Nature 2008;455:1061–8.
6. Rad R, Rad L, Wang W, Cadinanos J, Vassiliou G, Rice S, et al. PiggyBac transposon mutagenesis: a tool for cancer gene discovery in mice. Science 2010;330:1104–7.
7. Kamnasaran D, Qian B, Hawkins C, Stanford WL, Guha A. GATA6 is an astrocytoma tumor suppressor gene identified by gene trapping of mouse glioma model. Proc Natl Acad Sci U S A 2007;104:8053–58.
8. Collier LS, Adams DJ, Hackett CS, Bendzick LE, Akagi K, Davies MN, et al. Whole-body sleeping beauty mutagenesis can cause penetrant leukemia/lymphoma and rare high-grade glioma without associated embryonic lethality. Cancer Res 2009;69:8429–37.
9. Valente EM, Abou-Sleiman PM, Caputo V, Muqit MM, Harvey K, Gispert S, et al. Hereditary early-onset Parkinson's disease caused by mutations in PINK1. Science 2004;304:1158–60.
10. Gandhi S, Wood-Kaczmar A, Yao Z, Plun-Favreau H, Deas E, Klupsch K, et al. PINK1-associated Parkinson's disease is caused by neuronal vulnerability to calcium-induced cell death. Mol Cell 2009;33:627–38.
11. Wang X, Winter D, Ashrafi G, Schlehe J, Wong YL, Selkoe D, et al. PINK1 and Parkin target Miro for phosphorylation and degradation to arrest mitochondrial motility. Cell 2011;147:893–906.
12. Nogueira V, Park Y, Chen CC, Xu PZ, Chen ML, Tonic I, et al. Akt determines replicative senescence and oxidative or oncogenic premature senescence and sensitizes cells to oxidative apoptosis. Cancer Cell 2008;14:458–70.
13. Bensaad K, Cheung EC, Vousden KH. Modulation of intracellular ROS levels by TIGAR controls autophagy. EMBO J 2009;28:3015–26.
14. Gorrini C, Harris IS, Mak TW. Modulation of oxidative stress as an anticancer strategy. Nat Rev Drug Discov 2013;12:931–47.
15. Pollard SM, Yoshikawa K, Clarke ID, Danovi D, Stricker S, Russell R, et al. Glioma stem cell lines expanded in adherent culture have tumor-specific phenotypes and are suitable for chemical and genetic screens. Cell Stem Cell 2009;4:568–80.
16. Agnihotri S, Gajadhar AS, Ternamian C, Gorlia T, Diefes KL, Mischel PS, et al. Alkylpurine-DNA-N-glycosylase confers resistance to temozolomide in xenograft models of glioblastoma multiforme and is associated with poor survival in patients. J Clin Invest 2012;122:253–66.
17. Agnihotri S, Wolf A, Munoz DM, Smith CJ, Gajadhar A, Restrepo A, et al. A GATA4-regulated tumor suppressor network represses formation of malignant human astrocytomas. J Exp Med 2011;208:689–702.
18. Huang X, He Y, Dubuc AM, Hashizume R, Zhang W, Reimand J, et al. EAG2 potassium channel with evolutionarily conserved function as a brain tumor target. Nat Neurosci 2015;18:1236–46.
19. Wolf A, Agnihotri S, Micallef J, Mukherjee J, Sabha N, Cairns R, et al. Hexokinase 2 is a key mediator of aerobic glycolysis and promotes tumor growth in human glioblastoma multiforme. J Exp Med 2011;208:313–26.
20. Johansson FK, Goransson H, Westermark B. Expression analysis of genes involved in brain tumor progression driven by retroviral insertional mutagenesis in mice. Oncogene 2005;24:3896–905.
21. Song L, Huang Q, Chen K, Liu L, Lin C, Dai T, et al. miR-218 inhibits the invasive ability of glioma cells by direct downregulation of IKK-beta. Biochem Biophys Res Commun 2010;402:135–40.

22. Israelsen WJ, Dayton TL, Davidson SM, Fiske BP, Hosios AM, Bellinger G, et al. PKM2 isoform-specific deletion reveals a differential requirement for pyruvate kinase in tumor cells. Cell 2013;155:397–409.
23. Anastasiou D, Poulogiannis G, Asara JM, Boxer MB, Jiang JK, Shen M, et al. Inhibition of pyruvate kinase M2 by reactive oxygen species contributes to cellular antioxidant responses. Science 2011;334:1278–83.
24. Chandel NS, Maltepe E, Goldwasser E, Mathieu CE, Simon MC, Schumacker PT. Mitochondrial reactive oxygen species trigger hypoxia-induced transcription. Proc Natl Acad Sci U S A 1998;95:11715–20.
25. Chandel NS, McClintock DS, Feliciano CE, Wood TM, Melendez JA, Rodriguez AM, et al. Reactive oxygen species generated at mitochondrial complex III stabilize hypoxia-inducible factor-1alpha during hypoxia: a mechanism of O2 sensing. The Biol Chem 2000;275:25130–8.
26. Sarkaria JN, Carlson BL, Schroeder MA, Grogan P, Brown PD, Giannini C, et al. Use of an orthotopic xenograft model for assessing the effect of epidermal growth factor receptor amplification on glioblastoma radiation response. Clin Cancer Res 2006;12:2264–71.
27. Verhaak RG, Hoadley KA, Purdom E, Wang V, Qi Y, Wilkerson MD, et al. Integrated genomic analysis identifies clinically relevant subtypes of glioblastoma characterized by abnormalities in PDGFRA, IDH1, EGFR, and NF1. Cancer Cell 2010;17:98–110.
28. Ferber EC, Peck B, Delpuech O, Bell GP, East P, Schulze A. FOXO3a regulates reactive oxygen metabolism by inhibiting mitochondrial gene expression. Cell Death Differ 2012;19:968–79.
29. Hagenbuchner J, Ausserlechner MJ. Mitochondria and FOXO3: breath or die. Front Physiol 2013;4:147.
30. Read RD, Cavenee WK, Furnari FB, Thomas JB. A drosophila model for EGFR-Ras and PI3K-dependent human glioma. PLoS Genetics 2009;5: e1000374.
31. Madhavan S, Zenklusen JC, Kotliarov Y, Sahni H, Fine HA, Buetow K. Rembrandt: helping personalized medicine become a reality through integrative translational research. Mol Cancer Res 2009;7:157–67.
32. Cancer Genome Atlas Research N, Brat DJ, Verhaak RG, Aldape KD, Yung WK, Salama SR, et al. Comprehensive, Integrative Genomic Analysis of Diffuse Lower-Grade Gliomas. N Engl J Med 2015;372:2481–98.
33. Noushmehr H, Weisenberger DJ, Diefes K, Phillips HS, Pujara K, Berman BP, et al. Identification of a CpG island methylator phenotype that defines a distinct subgroup of glioma. Cancer Cell 2010;17:510–22.
34. Narendra DP, Jin SM, Tanaka A, Suen DF, Gautier CA, Shen J, et al. PINK1 is selectively stabilized on impaired mitochondria to activate Parkin. PLoS Biol 2010;8:e1000298.
35. Trachootham D, Alexandre J, Huang P. Targeting cancer cells by ROS-mediated mechanisms: a radical therapeutic approach? Nat Rev Drug Discov 2009;8:579–91.
36. Finley LW, Carracedo A, Lee J, Souza A, Egia A, Zhang J, et al. SIRT3 opposes reprogramming of cancer cell metabolism through HIF1alpha destabilization. Cancer Cell 2011;19:416–28.
37. Requejo-Aguilar R, Lopez-Fabuel I, Fernandez E, Martins LM, Almeida A, Bolanos JP. PINK1 deficiency sustains cell proliferation by reprogramming glucose metabolism through HIF1. Nat Commun 2014;5:4514.
38. Priyadarshini M, Tuimala J, Chen YC, Panula P. A zebrafish model of PINK1 deficiency reveals key pathway dysfunction including HIF signaling. Neurobiol Dis 2013;54:127–38.
39. Lim JH, Lee YM, Chun YS, Chen J, Kim JE, Park JW. Sirtuin 1 modulates cellular responses to hypoxia by deacetylating hypoxia-inducible factor 1alpha. Molecular cell 2010;38:864–78.
40. Zhong L, D'Urso A, Toiber D, Sebastian C, Henry RE, Vadysirisack DD, et al. The histone deacetylase Sirt6 regulates glucose homeostasis via Hif1alpha. Cell 2010;140:280–93.
41. Koh H, Kim H, Kim MJ, Park J, Lee HJ, Chung J. Silent information regulator 2 (Sir2) and Forkhead box O (FOXO) complement mitochondrial dysfunction and dopaminergic neuron loss in Drosophila PTEN-induced kinase 1 (PINK1) null mutant. J Biol Chem 2012;287:12750–8.
42. Mei Y, Zhang Y, Yamamoto K, Xie W, Mak TW, You H. FOXO3a-dependent regulation of Pink1 (Park6) mediates survival signaling in response to cytokine deprivation. Proc Natl Acad Sci U S A 2009;106:5153–8.
43. Trimmer C, Sotgia F, Whitaker-Menezes D, Balliet RM, Eaton G, Martinez-Outschoorn UE, et al. Caveolin-1 and mitochondrial SOD2 (MnSOD) function as tumor suppressors in the stromal microenvironment: a new genetically tractable model for human cancer associated fibroblasts. Cancer Bio Ther 2011;11:383–94.
44. Murata H, Sakaguchi M, Kataoka K, Huh NH. Multiple functions of PINK1 at different intracellular locations: beyond neurodegenerative diseases. Cell Cycle 2011;10:1518–9.
45. Hasson SA, Kane LA, Yamano K, Huang CH, Sliter DA, Buehler E, et al. High-content genome-wide RNAi screens identify regulators of parkin upstream of mitophagy. Nature 2013;504:291–5.
46. Choi I, Kim J, Jeong HK, Kim B, Jou I, Park SM, et al. PINK1 deficiency attenuates astrocyte proliferation through mitochondrial dysfunction, reduced AKT and increased p38 MAPK activation, and downregulation of EGFR. Glia 2013;61:800–12.
47. Sullivan LB, Chandel NS. Mitochondrial reactive oxygen species and cancer. Cancer Metab 2014;2:17.
48. Martin SA, Hewish M, Sims D, Lord CJ, Ashworth A. Parallel high-throughput RNA interference screens identify PINK1 as a potential therapeutic target for the treatment of DNA mismatch repair-deficient cancers. Cancer Res 2011;71:1836–48.
49. Bagchi A, Mills AA. The quest for the 1p36 tumor suppressor. Cancer Res 2008;68:2551–6.
50. Unoki M, Nakamura Y. Growth-suppressive effects of BPOZ and EGR2, two genes involved in the PTEN signaling pathway. Oncogene 2001;20:4457–65.
51. Berthier A, Navarro S, Jimenez-Sainz J, Rogla I, Ripoll F, Cervera J, et al. PINK1 displays tissue-specific subcellular location and regulates apoptosis and cell growth in breast cancer cells. Hum Pathol 2011;42:75–87.